# Straight Line Detection through Sub-pixel Hough Transform

Guillermo J. Bergues
Universidad Tecnológica Nacional
Facultad Regional Córdoba
Email: gjbergues@gmail.com

Clemar Schürrer
Universidad Tecnológica Nacional
Facultad Regional Córdoba
Email: cschurrer@gmail.com

Nancy Brambilla
Universidad Tecnológica Nacional
Facultad Regional Córdoba
Email: nancybrambilla@gmail.com

***Abstract*—In this study, we present the sub-pixel Hough Transform, which is used to detect line positions at sub-pixel level. A comparison with the conventional Hough Transform was performed. As a result, we obtained an increase in detection resolution.**

***Keywords*—Hough Transform; sub-pixel line detection; metrology**

## I. Purpose

The edges and lines that delimit objects in images are the most important features in pattern recognition. This natural aptitude of human beings is of great interest in the area of procedure automation via computer vision, especially when we aim at obtaining a certain measurement (of position or form) [1].

For a computer vision system to be able to emulate the measurements made by a specialized operator, it is necessary to recognize the global image based on simple patterns (lines, edges, circles). For example, one of the most interesting features of this approach is the ability to recognize the straight segments present in the graduated reticles of high-precision optical measuring instruments [2].

In most applications for line or contour detection, an edge detector is used. There are many edge detection methods; however, the most common ones have been designed based on discrete derivatives applied in the image seen as a surface [3]. Nevertheless, the position of the detected edges is approximate due to loss of information in the procedure. This is a serious problem if we are attempting at obtaining an exact measurement.

Given that modern vision systems require high precision and accuracy, the development of sub-pixel techniques for detecting lines and edges is one of the most interesting topics in dimensional metrology [4], [5]. In view of said matter, this paper presents the implementation of a line detection algorithm based on the Hough Transform. We introduce key modifications in the Hough transform in order to detect lines at sub-pixel level.

The conventional Hough transform [6] detects at a maximum resolution of $0.5$ pixels. To improve this resolution, we analyse a new parametric space given by $\rho(G) = x \cdot cos(\theta(G)) + y \cdot sin(\theta(G))$, where $(G)$ is each image gray level. $H_i$ accumulators are created, corresponding to each gray level, which are then derived into a four-dimensional density function. In its maximum peaks, this density function presents the positional information of each of the lines at sub-pixel level.

The overall algorithm performance was studied under a rigorous simulation of the lines present in the reticle of a high precision optical instrument (Nikon 6B Autocollimator) that includes the noise analysis.

## II. Background: Conventional Hough Transform

The Conventional Hough Transform (CHT) is a technique used to isolate features within an image. The curves in the image are parametrized as straight lines, polynomials and circles [6]. To achieve the objective, the CHT transforms the edged binary image's discrete space, defined by pixels, into the parametric space in function with the variables $\theta$ and $\rho$. These two parameters define a line through $\rho = x \cdot cos(\theta) + y \cdot sen(\theta)$. In this way, a set of properties is developed between the parametric and the image plane. These properties allow us to solve the problem of detecting a line in a binary image. Fig. 1 explains how the collinear points of the binary plane are transformed into a set of concurrent sinusoidal curves in the parametric plane.

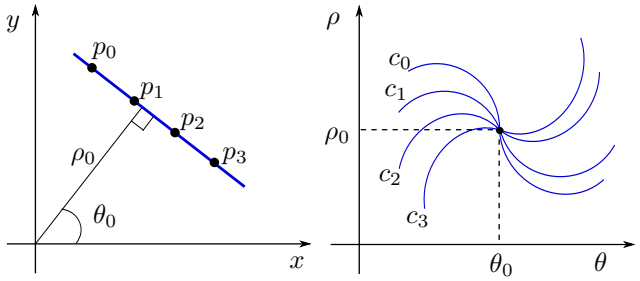


Fig. 1: Transformation of collinear points from a binary image $(x, y)$ to the parametric plane $(\theta, \rho)$.

### A. Edge detectors

The CHT algorithm works with an edge detector filter which allows the image plane to be transformed into a binary image plane. The most commonly used filters are Sobel and Canny, which include some pre-processing tasks to reduce the image noise [7], [8]. Being the mostly used filter, Canny poses a disadvantage: in addition to removing the noise, it blurs the image, causing the finest details to be lost [9, p.

176]. Therefore, Canny's Gaussian filter causes the CHT not to accurately detect line position, which generates a greater uncertainty in the measurement.

### *B. Simulation*

To determine the algorithms' detection accuracy, we used a simulation which represents the scale segments of a Nikon 6D autocollimator. In Fig. 2a, we can observe a line segment extracted from a real captured image and in Fig. 2b, a simulated segment. As a result, the real lines of both the instrument's cross and scale are represented [4]. And we introduce noise in every image using a signal-to-noise ratio (S/N) as a measure of it. The use of this simulated data enabled the analysis of each simulated detector's performance.

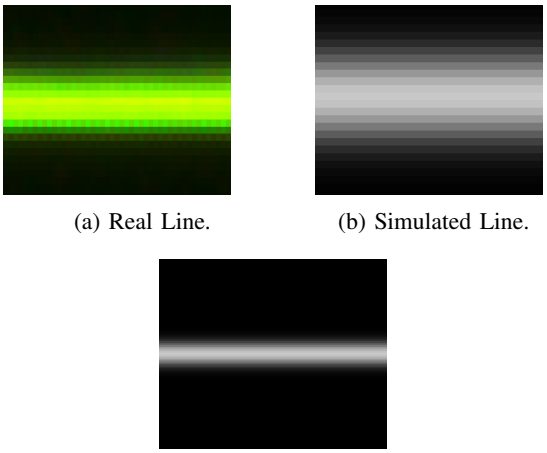

(a) Real Line. (b) Simulated Line.

(c) Simulated image.

Fig. 2: Segment of the real line $(a)$ and the simulated line $(b)$. Simulated image $(c)$.

The equation used to generate the Gaussian line in an image $I$ formed by a matrix $(N_x, N_y)$, was the following:

$$I(i,j) = round(A.e^{\frac{-(m-j)^2}{2.\Delta^2}}),\ i_0 = \frac{N_y}{2} \in N, \qquad (1)$$

The values of $c$ (position of the simulated line) to be estimated are $m = i_0 + k$ with $k = 1/100$. The $round$ function is the round to the nearest integer function. The width of the line given by $\Delta$ allows us to build a line according to the number of pixels that the line in the captured images occupies (using a BASLER ACA 1600/20gc camera as a model). Where:

$$0 \leq I(i,j) \leq 255\ e\ I(i,j) \in N, \qquad (2)$$

### *C. CHT Performance*

The Sobel filter is used in pre-processing because it is the one that is best suited for this type of images [4]. On the other hand, taking into account the sub-pixel centroid values $c'$ estimated for each detector as a linear function of the simulated centroids $c$, the Pearson correlation coefficient $r$ [10] is used as a quality estimation measurement.

In this first study, the line was moved at pixel level in the simulation image with integer values of $k = 1, ..., 100$ on (1) because the CHT doesn't detect at sub-pixel level. The results for a $S/N = 23dB$ are shown in Fig. 3; and in Table I, the detection under noise and its behaviour can be observed, using the Pearson coefficient as a measure.

TABLE I: $D_{H1}$: Pearson coefficient values for the different noise levels studied.

| S/N | $r_H$ |
|---|---|
| 1 dB | 0.18736 |
| 5 dB | 0.47941 |
| 10 dB | 0.95070 |
| 18 dB | 0.999 |
| 23 dB | 0.99999 |

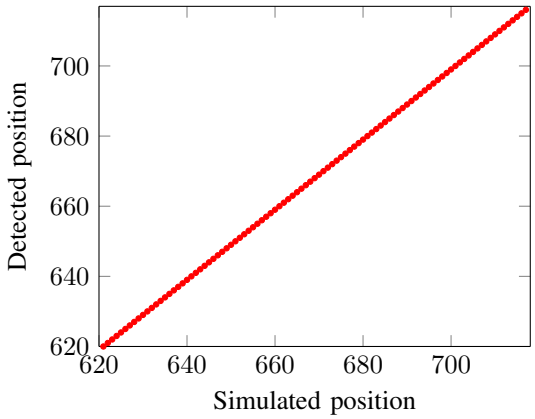


Fig. 3: CHT detector: Detected line position vs. simulated position (spacing between lines equals 1 pixel) $r \approx 0.999$, (with $S/N = 23dB$)

### *D. CHT Resolution*

Although the above results are correct for some applications, the CHT algorithm detects at sub-pixel level with a maximum resolution of $0.5$ pixels (at sub-pixel level, $k = 1/100$, there is not detection). On the other hand, if line thickness is formed by an even number of pixels, the transform chooses one of the two, according to its weight, introducing errors in the position measurement. This problem is schematized in Fig. 4, where the representation of the captured line of Fig. 2a is shown, with its respective central detection starting from the two edges that emerge from the filter.

## III. Method

In order to improve the resolution of $0.5$ pixels, it is not enough to apply any of the conventional detection methods that derive from the CHT, since similar results would be obtained again. This is so because in the CHT, the information contained in the gray levels is almost completely lost when the thresholding is performed to obtain the binary image (Sobel in our case). The pre-processing tasks, both thresholding and edge detection, are necessary in the CHT, but they can be ignored if a new parametric space is created. This new space has to include the intensity value given by each grey level [11]. This space, called "gray Hough parameter counting space", allows us to originally detect linear bands (of a single grey level) at the different intensity levels of the image. Each band is

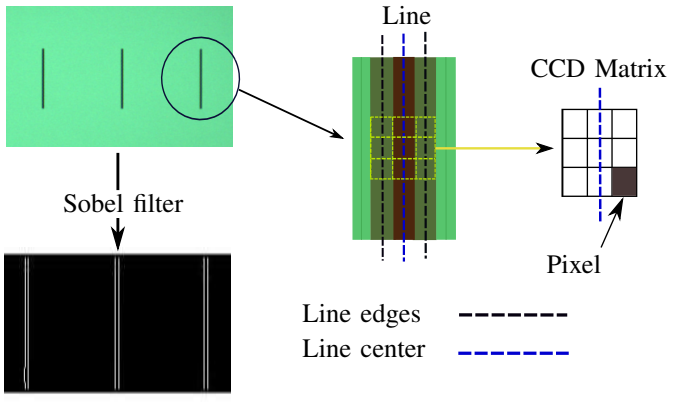


Fig. 4: Sub-pixel value of the detected line position. The pixel's central value of the CCD grid is taken from the edges detected by the Sobel filter. Maximum resolution value: $0.5$ pixels.

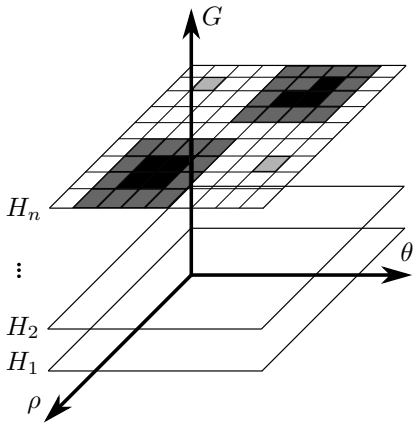


Fig. 5: Gray Hough parameter counting space. There is a sequence of $n$ matrices that form the $4D$ matrix. Each cell of matrix $H_n$ corresponds to a counting element for the gray level $n$.

defined as a parallel set of lines with the same orientation and grey level, whose main characteristics to obtain are: gray level, orientation, total number of pixels and length.

This highly useful approach for applications such as robotics and industrial processes is not suitable for measurements where the line position must be obtained with sub-pixel precision (not the band, but the central position of the band). On the other hand, the lines analysed are made up, in most cases, by several grey levels at the same time.

### A. *Sub-pixel Hough Transform*

Based on $\rho = x \cdot cos(\theta) + y \cdot sen(\theta)$, with an image space given by $(x, y, G)$, in which $G$ is the gray level corresponding to each point $(x, y)$ of the image, a new parametric space is formed:

$$\rho(G) = x \cdot cos(\theta(G)) + y \cdot sen(\theta(G)), \tag{3}$$

This parametric space defines a mapping space $f : (x, y, G) \rightarrow H(\rho, \theta, G)$ which builds $H_i$ accumulators that correspond to each gray level. $2^{n^\circ bits}$ accumulators -unified in a 4D matrix- are created, being $n$ the quantization bits number of the camera.

The $4D$ matrix behaves as an easy-to-understand density function: its maximums define the position of the lines in the space $(x, y)$. In Fig. 5, as an example, the local maximum values of the $H_n$ accumulator are shown. Black color responds to the region most likely to encounter a straight line for the gray level $n$.

It is important to emphasize that the CHT works with a single accumulator $H$ that includes all the information corresponding to the number of lines in the image and, therefore, all the information that is discarded in the thresholding stage is lost. The new parametric space does not lose relevant information for line positioning.

The following algorithm summarizes the procedure:

1) Initialize each accumulator $H(\rho, \theta, G)$ a 0.
2) For each pixel $(x, y, G)$ y $\theta_j = 0^\circ \rightarrow 179^\circ$.
3) Calculate $\rho_j(G_i) = x_i \cdot cos(\theta_j(G_i)) + y_i \cdot sen(\theta_j(G_i))$.
4) $H(\rho_j, \theta_j, G_i) = H(\rho_j, \theta_j, G_i) + 1$.
5) Create the final matrix $H_T = H_1 + ... + H_n$.
6) Compute the points with the highest degree of probability in the parametric plane.
7) Map these points onto the image plane and obtain the density function center that is defined by them.

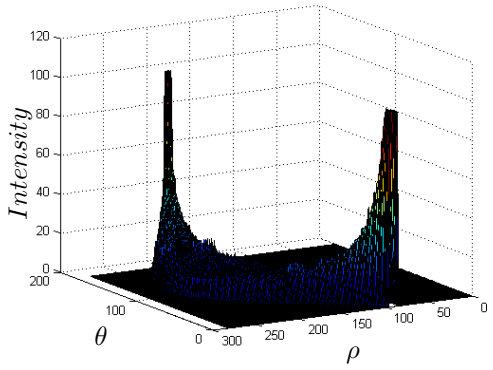


Fig. 6: Density function of final parametric plane. It is obtained from the sum $H_T = H_1 + ... + H_n$. The peaks present in the density function correspond to the searched lines' centers.

From a geometric structure point of view, the lines are composed of several connected parallel straight lines, which have an equal $\theta$ orientation, have different distances $\rho_i$ and different gray levels (see Fig. 2b). Once the transformation to gray levels is performed, each of these lines is mapped onto a local maximum in its respective accumulator $H_i$ (as in accumulator $H_n$ of Fig. 5). These maximum values are forming the peaks shown in Fig. 6, which are then searched to obtain the center of the line in the pixels plane $(x, y)$.

### B. *Results*

Table II shows the results of the Pearson coefficients calculated for the different noise levels studied. Fig. 7 shows the relationship between the simulated positions and those

obtained by the Hough sub-pixel detector (with $S/N = 23dB$). Each noise level has a similar curve. On the other hand, Fig. 8 is a summary of the sub-pixel detector study. It shows the relationship between the signal-to-noise ratio $S/N$ and its $r$ value.

TABLE II: Sub-pixel Hough transform: Pearson coefficient values for the different noise levels studied.

| S/N | $r_H$ |
|---|---|
| 13 dB | 0.9494 |
| 14 dB | 0.9512 |
| 15 dB | 0.9518 |
| 16 dB | 0.9579 |
| 17 dB | 0.9645 |
| 18 dB | 09669 |
| 19 dB | 0.9748 |
| 20 dB | 0.9804 |
| 21 dB | 0.9811 |
| 22 dB | 0.9821 |
| 23 dB | 0.9846 |

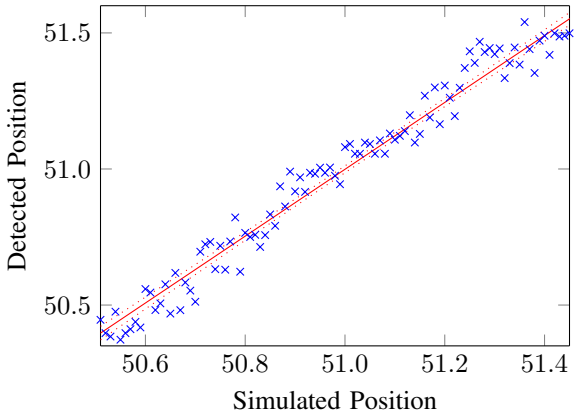


Fig. 7: Sub-pixel Hough Detection: Detected position vs. Simulated position. $r = 0.9846$ ($S/N = 23dB$).

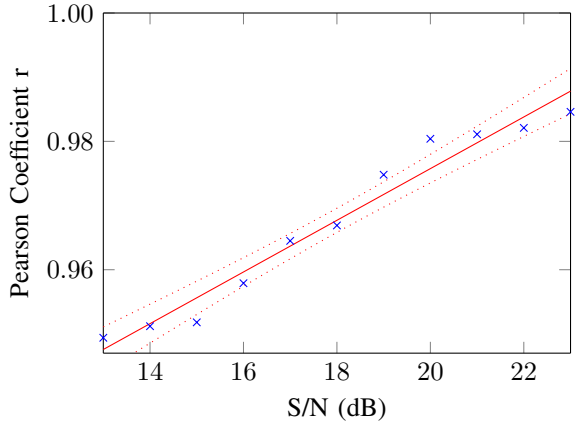


Fig. 8: Sub-pixel Hough detection: r vs. S/N.

## IV. Conclusions

After analysing Fig. 8, it is clearly seen that, as the $S/N$ increases, sub-pixel detection is better ($r$ approaches the ideal value 1). There is a fairly linear growth that stops in $20dB$ and remains on a slightly positive slope's plateau. This behaviour is so due to the fact that the density function represents a part of all the information on the positions of the lines. The detector has an operating stop around the value of $r = 0.9850$.

Another important fact that emerges from the analysis of the curves is that the dispersion degree of the data, according to the regression line, is very good. The average quadratic dispersion $(s)$ is equal to 0.05 pixels using a BASLER ACA 1600 20gc camera as a model for the simulation.

As a main result, this new algorithm allows for line detection at sub-pixel level, being this 10 times better in resolution than the CHT (which detects at a maximum resolution of 0.5 pixels). Moreover, this new algorithm does not depend on an odd pixel structure like the CHT. On the other hand, this maximum value is tied to the characteristics of the camera ($n^\circ$ of bits and resolution). If these latter values increase, the new parametric space can be more detailed and therefore a higher resolution can be obtained.

## References

[1] L. Fernandes, M. Oliveira, and R. Silva, *Uncertainty Propagation: Avoiding the Expensive Sampling Process for Real-time Image-based Measurements*, Comput. Stat. Data Anal., vol. 52, no. 7, pp. 3852–3876, 2008.

[2] G. Bergues, G. Ames, L. Canali, C. Schurrer, and A. Flesia,*External visual interface for a Nikon 6d autocollimator*, in Instrumentation and Measurement Technology Conference (I2MTC) Proceedings, 2014 IEEE International, pp. 35–39, May 2014.

[3] R. Maini and H. Aggarwal, *Study and comparison of various image edge detection techniques*, International journal of image processing (IJIP), vol. 3, no. 1, pp. 1-11, 2009.

[4] A.G. Flesia, G. Ames, G. Bergues, L. Canali, and C. Schurrer, *Sub-pixel straight lines detection for measuring through machine vision*, in Instrumentation and Measurement Technology Conference (I2MTC) Proceedings, 2014 IEEE International, pp. 402–406, May 2014.

[5] A. Fabijanska and D. Sankowski, *Computer vision system for high temperature measurements of surface properties*, Machine Vision and Applications, vol. 20, no. 6, pp. 411-421, 2009.

[6] R.O. Duda and P.E. Hart, *Use of the Hough Transformation to Detect Lines and Curves in Pictures*, ACM, vol. 15, no. 1, pp. 11-15, 1972.

[7] N. Senthilkumaran and R. Rajesh, *Edge detection techniques for image segmentation–a survey of soft computing approaches*, International Journal of Recent Trends in Engineering, vol. 1, no. 2, 2009.

[8] J. Canny, *A Computational Approach to Edge Detection*, Pattern Analysis and Machine Intelligence, IEEE Transactions on, vol. PAMI-8, n. 6, pp. 679-698, 1986.

[9] R. Gonzalez and R.E. Woods, *Digital image processing*, Prentice Hall Upper Saddle River, NJ, pp. 176-178, 2002.

[10] E.B. Niven and C.V. Deutsch,*Calculating a robust correlation coefficient and quantifying its uncertainty*, Computers and Geosciences, vol. 40, no. 0, pp. 1-9, 2012.

[11] R.C. Lo and W.H. Tsai, *Gray-scale hough transform for thick line detection in gray-scale images*, Pattern Recognition, vol. 28, no. 5, pp. 647-661, 1995.

[12] G. J. Bergues, C. Schürrer and N. Brambilla, *Uncertainty Determination of the Set Nikon 6B Autocollimator + Visual Interface*, in IEEE Transactions on Instrumentation and Measurement, vol. 67, no. 5, pp. 1058-1064, May 2018.